Extracting electronic many-body correlations from local measurements with artificial neural networks

Faluke Aikebaier[1,2,3], Teemu Ojanen[1,2] and Jose L. Lado[3]

1 Computational Physics Laboratory, Physics Unit, Faculty of Engineering and Natural Sciences, Tampere University, FI-33014 Tampere, Finland
2 Helsinki Institute of Physics P.O. Box 64, FI-00014, Finland
3 Department of Applied Physics, Aalto University, 00076, Espoo, Finland

Abstract

The characterization of many-body correlations provides a powerful tool for analyzing correlated quantum materials. However, experimental extraction of quantum entanglement in correlated electronic systems remains an open problem in practice. In particular, the correlation entropy quantifies the strength of quantum correlations in interacting electronic systems, yet it requires measuring all the single-particle correlators of a macroscopic sample. To circumvent this bottleneck, we introduce a strategy to obtain the correlation entropy of electronic systems solely from a set of local measurements. We show that, by combining local particle-particle and density-density correlations with a neural-network algorithm, the correlation entropy can be predicted accurately. Specifically, we show that for a generalized interacting fermionic model, our algorithm yields an accurate prediction of the correlation entropy from a set of noisy local correlators. Our work shows that the correlation entropy in interacting electron systems can be reconstructed from local measurements, providing a starting point to experimentally extract many-body correlations with local probes.

Contents

1 Introduction

Quantum correlation between interacting particles is one of the most fundamental aspects of many-body theory [1]. The strength of quantum correlations quantifies the complexity of a many-body state with respect to a product state of non-interacting particles [2–6]. Specifically, non-interacting fermionic systems are described by Slater determinant states with vanishing multi-particle entanglement. While highly correlated states emerge from many-body electronic interactions, strong interactions may or may not guarantee strong quantum many-body correlations. In particular, while some quantum states are faithfully captured by a mean-field theory [7, 8], more exotic correlated states inherently emerge from non-trivial quantum correlations [9, 10]. In this spirit, many-body entanglement provides a powerful framework to classify emergent properties of quantum materials [11, 12]. However, direct experimental probes of entanglement remain very limited [13].

Quantum correlations in a many-body state can be quantified by different entanglement measures, including the bipartite von Neumann and Renyi entropies of the density matrix [14–16]. These quantities characterize quantum correlations between two arbitrarily chosen disjoint partitions of a system, yet importantly, are non-zero even for non-interacting electronic systems [17–20]. Instead, to quantify entanglement in fermionic systems, it is natural to adopt the von Neumann entropy associated with the correlation matrix, or one-particle density matrix (ODM) [21–24], which identically vanishes in the non-interacting limit. The correlation entropy has been theoretically studied in various fermionic systems [25–30], however, it has not been experimentally measured up to date. Such measurement would require extracting two-point correlations in the whole system, which is unfeasible for thermodynamically large systems.

Here we address the gap between theory and experiments in electronic many-body entanglement by designing a methodology based on an artificial neural network algorithm to obtain the correlation entropy from minimal local measurement data. Artificial neural-network algorithms are new tools for solving physics problems and have been applied to quantum many-body physics [31–34]. In supervised learning with artificial neural networks, the model is trained on data consisting of labeled examples in which a certain input data is mapped to an output [35]. By learning the relationship between the input data and the output, the model can predict outputs from new data for quantum systems similar to the training set [35]. This approach is especially useful for predicting an observable challenge to measure, such as the correlation entropy, using as input accessible quantities like local correlators, as illustrated in Fig. 1(a). The input data for the algorithm constitutes particle-particle and density-density correlation functions on a set of sites. The neural-network algorithm allows extracting the correlation entropy from the set of local measurements. Ultimately, if obtained experimentally, this would allow extraction of the correlation entropy of the physical system. We demonstrate this methodology by analyzing a generalized interacting model incorporating local and non-local interactions, spin-orbit coupling, and magnetic fields. It is worth noting that our methodology is demonstrated only for a generalized family of one-dimensional models. The extension to two-dimensional models would require retraining with additional data and a potential slight change in the architecture of the algorithm. For the family of models we consider, we show that our procedure is robust to noise in the input data, providing a promising strategy

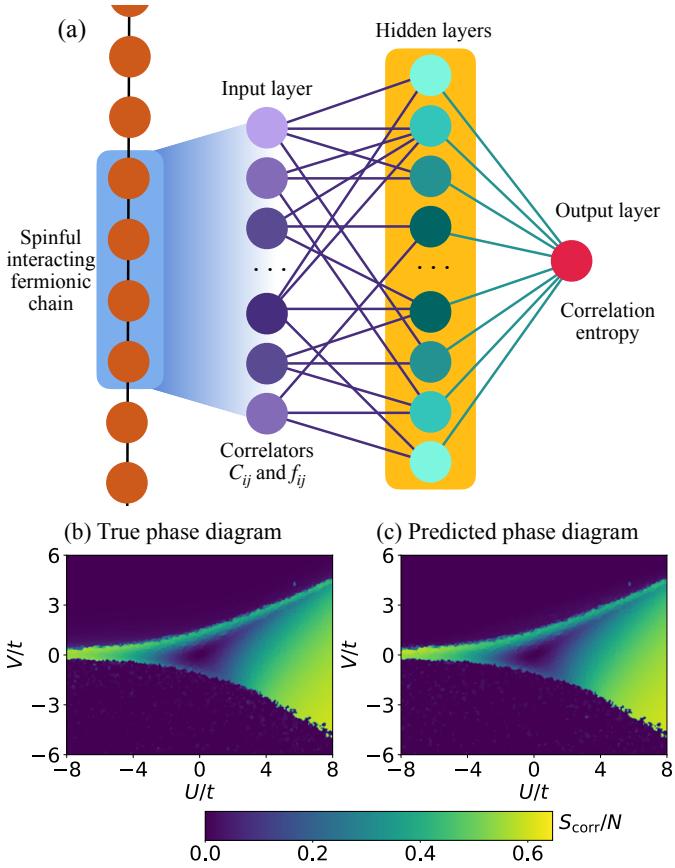

Figure 1: The neural-network structure and the phase diagram of the correlation entropy. (a) Schematic of a one-dimensional interacting fermionic system, where a set of local measurements allow extracting the correlation entropy through a trained neural-network algorithm. (b) The UV-phase diagram of the correlation entropy. (c) The neural-network model predicted the UV-phase diagram of the correlation entropy.

to characterize the strength of many-body correlations in interacting electronic systems.

2 Model

Before addressing our approach based on local measurements, we first illustrate how the correlation entropy can be computed theoretically [Fig. 1(b)], where we have access to all the non-local correlation functions. In the following, we take the correlation entropy as the characteristic measure of the strength of many-body entanglement in fermionic systems. Correlation entropy is a type of many-body fermionic entanglement entropy similar to partition entanglement entropy in spin systems. The correlation entropy in a fermionic many-body state $|\Psi_0\rangle$ is defined in terms of the correlation matrix

$$C_{ij}^{ss'} = \langle\Psi_0|c_{is}^\dagger c_{js'}|\Psi_0\rangle, \tag{1}$$

where c_{is}, $c_{is}^\dagger$ are the annihilation and creation operators at site i and spin s. For a system with N spinful sites, the correlation matrix has dimensions $2N \times 2N$. Due to the Fermi statistics, the eigenvalues α_i of the correlation matrix satisfy $0 \leq \alpha_i \leq 1$. The definition in Eq. (1) is similar to the Green's function matrix, but the convenience of the correlation matrix allows us

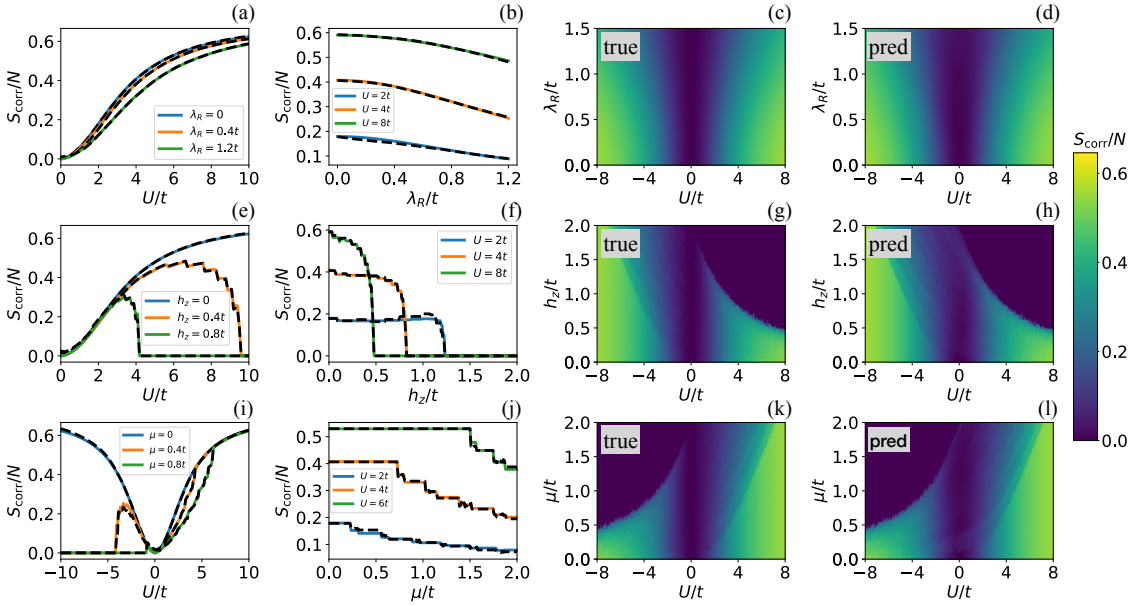

Figure 2: Correlation entropy for the generalized interacting model in the limit $V = t' = 0$. Dashed lines correspond to neural-network prediction and solid lines to the real value of the correlation entropy. Dependence of S_{corr} on the on-site interaction U for various values of λ_R in (a), for various values of h_z in (e), and for various values of μ in (i). Dependence of S_{corr} on λ_R in (b), on h_z in (f), and on μ in (j) for various values of U. Panels (c,g,k) show the real correlation entropy and (d,h,l) the neural-network prediction based on local measurements, in the plane $\lambda_R U$ (c,d), $h_z U$ (g,h), and μU (k,l).

to define the correlation entropy as

$$S_{\text{corr}} = -\sum_{j=1}^{2N} \alpha_j \log \alpha_j, \tag{2}$$

which is non-negative and, in contrast to partition entanglement entropies [14], scales linearly in the system size even in ground states of local Hamiltonians. The correlation entropy is a measure of fermionic entanglement in the following sense. If there exists a single-particle basis in which the many-body state can be written as a product state $|\Psi_0\rangle = \prod_j \hat{c}_j^\dagger |0\rangle$, also known as a Slater determinant, then all the eigenvalues of the correlation matrix are either 0 or 1 and the correlation entropy vanishes. A nonzero value of the correlation entropy implies an obstruction of finding a basis where $|\Psi_0\rangle$ can be written as a single product state, thus implying finite multi-particle entanglement. In a non-interacting system, the full many-body wavefunction can always be written as a product state in the diagonal single-particle bases. It is necessary to have finite many-body interactions to produce eigenstates with positive correlation entropy. However, stronger interactions do not necessarily imply larger correlation entropy, as interactions can also drive a system towards a symmetry-broken product state. The correlation entropy is thus a measure of how far away a given state is from a single product state. Thus, it is a measure of quantum complexity rather than a measure of the strength of interactions. As a proxy to many-body correlations, the correlation entropy is qualitatively different from bipartite entanglement entropies [36, 37]. Despite the fact that correlation matrices also play a role in calculating free fermion bipartite entanglement entropies [38], the correlation entropy and partition entropies characterize the fundamentally different types of quantum correlations. In particular, the partition entanglement entropies are nonzero even

for free fermion systems [17–19], in contrast to the correlation entropy.

To make the previous discussion concrete, we consider a one-dimensional generalized model of spinful interacting fermions of the form

$$\begin{aligned} H = &-t\sum_{j,s}\left(c^\dagger_{j,s}c_{j+1,s}\right) + t'\sum_{j,s}\left(c^\dagger_{j,s}c_{j+2,s}\right) \\ &-\mu\sum_j\left(n_{j,\uparrow}+n_{j,\downarrow}\right) + h_z\sum_{j,s,s'}c^\dagger_{j,s}\sigma_z^{s,s'}c_{j,s'} \\ &+U\sum_j\left(n_{j,\uparrow}-\frac{1}{2}\right)\left(n_{j,\downarrow}-\frac{1}{2}\right) \\ &+V\sum_j\left(n_{j,\uparrow}+n_{j,\downarrow}-1\right)\left(n_{j+1,\uparrow}+n_{j+1,\downarrow}-1\right) \\ &+i\lambda_R\sum_{\langle jk\rangle ss'}c^\dagger_{j,s}\left(\boldsymbol{\sigma}_{ss'}\times\boldsymbol{d}_{jk}\right)_z c_{k,s'} + \text{h.c.}, \end{aligned} \tag{3}$$

where $n_{j,s} = c^\dagger_{j,s}c_{j,s}$ is the number operator with spin s. The previous family of models has specific limits to non-interacting models, the one-dimensional Hubbard model, and the one-dimensional $t-V$ model, among others. Our procedure can be carried out in any subset of those models, yet for the sake of generality, we demonstrate our algorithm in a wide family of models. We also note that more complex generalized models could also be considered. The parameters t, t' control the first and second nearest-neighbour hopping, μ the chemical potential, U the on-site Hubbard many-body interaction, V the nearest-neighbour electronic many-body interaction, h_z the magnetic field in the z-direction, λ_R the Rashba spin-orbit coupling (SOC), $\boldsymbol{d}_{jk} = \boldsymbol{r}_j - \boldsymbol{r}_k$ with $\boldsymbol{r}_j$ the location of site j, $\langle jk\rangle$ denotes first neighboring sites, and $\boldsymbol{\sigma} = (\sigma_x, \sigma_y, \sigma_z)$ are the spin Pauli matrices. We find the ground state of Eq. (3) using the tensor-network formalism [39–42], which allows extracting the different two-point correlators in the full system and evaluating the correlation entropy. Below we consider finite systems with 24 lattice sites to generate phase diagrams and the training data for the neural network. As mentioned above, the correlation entropy is an extensive quantity. Therefore we consider the correlation entropy density, which becomes system-size independent for sufficiently large systems $L \gtrsim 20$. The system size dependence of the correlation entropy density is further discussed in Appendix 8.1. The employed systems with 24 sites are thus observed to accurately reproduce the phase diagram of the Hubbard model in the thermodynamic limit.

3 Results

3.1 Correlation entropy for extended Hubbard model

The correlation entropy in the UV-plane is presented in Fig. 1(b) and reproduces the essential features of the phase diagram as obtained from the von Neumann entanglement entropy [15, 17, 19, 20, 43–46]. For strong interactions $U, V \gg t$, the UV-phase show three different phases, charge-density wave, spin density wave, and a phase separation [15, 17, 19, 20, 43–46]. The observation of distinct phases in the phase diagram demonstrates that the correlation entropy allows identifying different correlated states. As expected, for vanishing interactions $U = 0$ and $V = 0$, the correlation entropy vanishes. The on-site interaction U acts as the main driver of the correlation entropy which saturates to the value $\ln 2$ per site at large $|U|$ [27]. In contrast, a strong nearest neighbor coupling V tends to suppress quantum correlations. The reason for this is that V promotes a charge density wave state for $V > 0$ and a phase-separated state for $V < 0$, both of which are described by a product state for large $|V|$ [17, 19, 20, 47]. While

both of these states are drastically different from the non-interacting ground state, they do not support sizable many-body quantum entanglement, as indicated by the vanishing correlation entropy.

3.2 Inferring correlation entropy from local measurements

Having established the main features of the correlation entropy in our model, we now present how to extract from a limited set of measurements. The central idea relies on reverse-engineering the correlation entropy from a small number of local correlation functions [48–54]. The many-body entanglement entropy is notoriously difficult to access in experiments [55] and measuring the correlation entropy faces similar challenges as it would require knowledge of the full correlation matrix [56]. With access to the full correlation matrix, the correlation entropy can be directly computed. However, this is experimentally unfeasible for large systems. This limitation motivates finding a complementary strategy involving correlations only between a limited number of lattice sites. In the following, we show that correlations in a few sites are sufficient to reverse-engineer the correlation entropy using a deep learning approach.

A schematic of our methodology is shown in Fig. 1(a). The input layer corresponds to a set of correlation functions of the spinful interacting fermionic chain measured locally. As inputs, we consider single-particle correlators in Eq. (1) and density-density correlators

$$f_{ij}^{ss'} = \langle \Psi_0 | n_{is} n_{js'} | \Psi_0 \rangle \tag{4}$$

evaluated on the four sites at the center of the chain. The indexes i, j in the correlators run over the four neighboring sites in the center of the chain. Our algorithm combines both types of correlators in the supervised learning algorithm, as the two types of correlators provide complementary information about the many-body state [57]. Details of the neural network architecture can be found in Methods. Crucially, we note that the neural network algorithm employing the training data from the 24-site chain already accurately reproduces the correlation entropy in the thermodynamic limit. Therefore, to apply the method to thermodynamically large systems, it is still sufficient to use input data from four adjacent sites and train the algorithm with only a 24-site model. This summarizes the remarkable power of the algorithm: the size of the subsystem from which the input data is obtained and the size of the system used for the training the algorithm does not scale as the size of the physical system which can be macroscopic.

As a specific benchmark, we first consider a minimal model with only nonzero $\{t, U, V\}$ in Eq. (3), which corresponds to the usual one-dimensional Hubbard model. As shown in Fig. 1(c), the machine learning prediction reproduces the exact results with high accuracy. Similarly, we also apply this methodology to an interacting model with Hubbard interaction, SOC, magnetic field, and doping separately. The results are shown in Fig. 2. In the left two columns, the dependence of U and other parameters on the correlation entropy are given with the prediction of the neural network model as the black dashed curves. We can see that the prediction of the neural network model captures well the features of the correlation entropy in the different regimes, as shown in the right-most column in Fig. 2. These results show the flexibility and accuracy of our methodology for various regimes of the interacting model.

3.3 Reconstructions from partial correlators and robustness to noise

In the section above we showed that the deep learning approach provides accurate results for special cases of Eq. (3) using simultaneously two-point and four-point correlators. However, experimentally, extracting one of the two sets of correlators may be more challenging than the other in specific setups. Furthermore, in experimentally realistic scenarios, the extracted correlators are expected to have a finite amount of noise. To address those challenges, here we

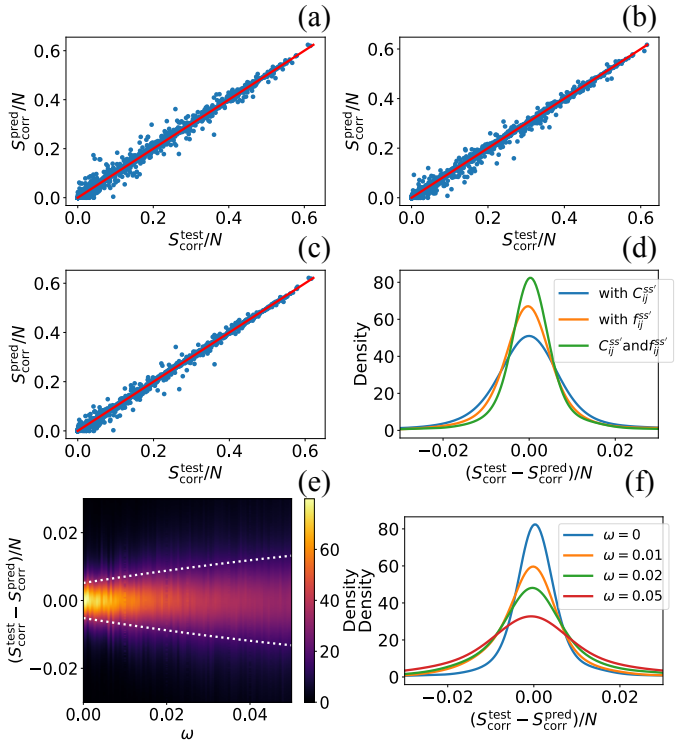

Figure 3: Predictions of the neural-network algorithm on the generalized interacting model in Eq. (3). (a) Predictions of the model trained with particle-particle correlators $C^{ss'}_{ij}$. (b) Predictions of the model trained with density-density correlators $f^{ss'}_{ij}$. (c) Predictions of the model trained on both $C^{ss'}_{ij}$ and $f^{ss'}_{ij}$. (d) Probability distribution of the difference between the predicted entropy from local measurements and the true one $S^{\rm test}_{\rm corr} - S^{\rm pred}_{\rm corr}$ in (a,b,c). (e) Probability distribution of the error in the prediction in the presence of noise. The half-band width of the probability distribution is depicted as a white dotted curve. (f) Probability distribution of the error in the prediction for particular noise rates.

show how this algorithm can be implemented with either two-point or four-point correlators separately, and that it is robust to noisy data.

We first consider the full model in Eq. (3) and a supervised algorithm that has been trained separately with local two-point correlators $C^{ss'}_{ij}$ or four-point density-density correlators $f^{ss'}_{ij}$. The results are shown in Fig. 3(a) and (b), highlighting a good agreement between the true end predicted correlation entropies. Both types of local correlators lead to comparable accuracy, yet lower than the model trained in both. The neural network model trained on both two-point $C^{ss'}_{ij}$ and four-point $f^{ss'}_{ij}$ correlation functions is shown in Fig. 3(c). This leads to a higher accuracy compared to the cases with only a single type of input data. A more quantitative comparison, a probability distribution [1] of the error between the true and predicted results, is shown in Fig. 3(d). We observe that the most accurate results are obtained with the network trained on both $C^{ss'}_{ij}$ and $f^{ss'}_{ij}$, leading to a typical error of 1%.

The robustness of the neural-network model can be benchmarked by introducing random noise in the data. For every different realization, we consider a different random noise that modifies every single correlator $\Lambda^{ss',0}_{ij} = \{C^{ss'}_{ij}, f^{ss'}_{ij}\}$ independently as

$$\Lambda^{ss'}_{ij} = \Lambda^{ss',0}_{ij} + \chi^{ss'}_{ij}, \tag{5}$$

[1] The probability distribution is computed with kernel density estimation algorithm

with $\Lambda_{ij}^{ss',0}$ the original correlators, $\Lambda_{ij}^{ss'}$ the noisy correlators, $\chi_{ij}^{ss'}$ the random noise between $[-\omega,\omega]$, and ω controlling the amplitude of the noise. A heat plot of the probability distribution of the error of the prediction of the neural network model is shown in Fig. 3(e). The probability distribution for particular values of ω is shown in Fig. 3(f). We can see that the neural network model is robust for a noise rate up to $\omega = 0.02$. The accuracy is comparable with the model trained in the absence of numerical noise. For stronger noise up to $\omega = 0.05$, the neural-network model predicts the correlation entropy within the error of 1.5%. The model performance in the presence of strong noise is discussed in Appendix 8.2

Obtaining information on multi-particle quantum correlations and entanglement with experimental probes is, in general, prohibitively challenging due to the large number of correlators that should be measured. With the machine learning algorithm introduced above, the correlation entropy can be deduced from correlation functions on a handful of lattice sites. Our results show that the correlation entropy for the macroscopically large systems can be extracted using local correlators obtained in a small number of lattice sites (four sites here) as the input. In particular, for a non-interacting system, the correlation entropy is identically zero, and thus our methodology allows characterizing the correlations stemming purely from many-body interactions. From the physical point of view, single-particle correlators can be directly inferred from non-local transport measurements [58, 59]. Spin-resolution in the correlators can be directly obtained by using spin-polarized leads [60, 61]. Regarding four-point correlators, our method employs density-density correlators that can be directly extracted from Friedel oscillations of the electronic charge when impurities are deposited on a single site [62, 63]. Analogously, spin-resolution could be achieved by employing magnetic impurities [64, 65].

4 Summary

To summarize, we proposed a supervised learning approach that allows quantitatively extracting bulk quantum correlations in interacting fermionic many-body systems from local measurements. Focusing on a generalized interacting spinful model, we demonstrated that the correlation entropy can be accurately inferred from a modest set of bulk measurements. The mapping between the local correlators and the correlation entropy is implemented with a neural-network algorithm. Furthermore, we demonstrated that this strategy can be implemented with two-point correlators, four-point-correlators, and both, providing a flexible strategy that can be adapted to different experimental setups. Finally, we demonstrated that this algorithm is robust to noise in the measurements, highlighting its feasibility for applications to experimental data. Our work provides a starting point to quantitatively characterize quantum correlation from experimental data in electronic systems, allowing us to map the degree of quantum entanglement from local measurements in quantum materials.

5 Methods

Here we discuss the architecture of the neural network used, that were implemented with Keras [66]. Accounting for spin, for each set of parameters $\{t, t', \mu, U, V, h_z, \lambda_R\}$, the input layer consists of 32 one particle correlators $C_{ij}^{ss'}$ and 32 density-density correlators $f_{ij}^{ss'}$. The training data is obtained by randomly generating 12,000 examples for sets of parameters $\{t, t', \mu, U, V, h_z, \lambda_R\}$ of a 24-site spinful interacting fermionic chain. After solving the ground state for each set of parameters, we can evaluate the correlators which are used as the input data, as well as the resulting correlation entropy in Eq. (2) employed as the target value for the supervised learning algorithm. We consider three hidden layers in the architecture with the

sequence of nodes 1024/2048/1024, which leads to the output layer, the correlation entropy. We choose the Adam algorithm for the optimizer, with the learning rate 5×10^{-5}, and mean absolute error as the loss function. We target the validation loss below 0.005 in the training process which results in similar accuracy on the test set. The neural-network architecture can be found in Zenodo [67].

We now elaborate on the many-body algorithms used. Many-body calculations were performed using the tensor-network matrix-product state (MPS) formalism implemented in dmrgpy [42], based on ITensor [40, 41]. Correlators are performed with full tensor contraction of the MPS [68] and ground states are computed with the density-matrix renormalization algorithm [39]. The spinful many-body fermionic problem is mapped to a spin problem using a spinful Jordan-Wigner transformation with Jordan-Wigner strings. The data generation based on tensor networks can be found in Zenodo [67].

We also note that there are no conceptual obstacles for our approach to be applied to 2d models in the future. The major challenge in this situation is to generate the training data, which requires a methodology to solve a relatively large two-dimensional interacting model. While some specific models can be solved using Quantum Monte Carlo solvers, generic models would present the sign problems, limiting the training systems that could be generated. It is worth noting that future development of neural-network quantum states may allow solving a generic set of interacting fermionic models, that would allow generating our training data. In contrast, for interacting one-dimensional systems, we could solve a generic large set of models using matrix-product states, allowing us to generate all the required training data.

6 Code availability

The data and codes implementing the data generation and training are available in Zenodo [67].

7 Acknowledgements

JLL acknowledges the financial support from the Academy of Finland Projects No. 331342 and No. 336243 and the Jane and Aatos Erkko Foundation. T.O. acknowledges the Academy of Finland project 331094 for support. FA acknowledges the financial support from the Magnus Ehrnrooth foundation. FA and JLL acknowledge the computational resources provided by the Aalto Science-IT project. We thank R. Koch for the useful discussions.

8 Appendix

8.1 System size dependence of the correlation entropy density

In this paper, the neural network model is trained on 24 sites interacting fermionic chain, with input data from 4 lattice sites in the center. The finite-size dependence of the correlation entropy density on the system size is shown in Fig. 4. If the physical system is very small, finite-size effects would play a role and potentially impact the prediction of the correlation entropy. The model trained on sites $L \gtrsim 20$ can accurately reproduce S_{corr}/N for thermodynamically large systems. Our focus is on systems that have converged towards the thermodynamic limit, where such finite-size effects are not dominating. Hence we can say that the correlation entropy density S_{corr}/N is system-size independent for systems with $L \gtrsim 20$ sites.

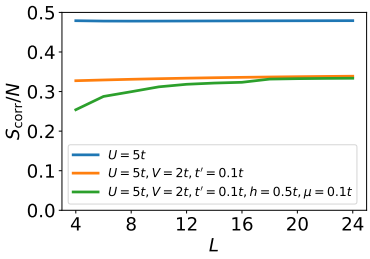

Figure 4: Correlation entropy as a function of different chain sizes. Three sets of parameters are used in the calculations for comparison.

8.2 Performance of the neural network model in the presence of strong noise

In this section, we examine the performance of the neural network model in the presence of strong noise. For this purpose, we introduce the noise rate up to $\omega = 0.3$, and show the results in Fig. 5. As can be observed in Fig. 5(a), the neural network model predicts the correlation entropy within the error of 2% up to $\omega = 0.1$. Further increasing the noise rate quickly reduces the accuracy of the model. In terms of the degree of the correlation, the effect of noise is stronger for smaller values of correlation entropy as shown in Fig. 5(b).

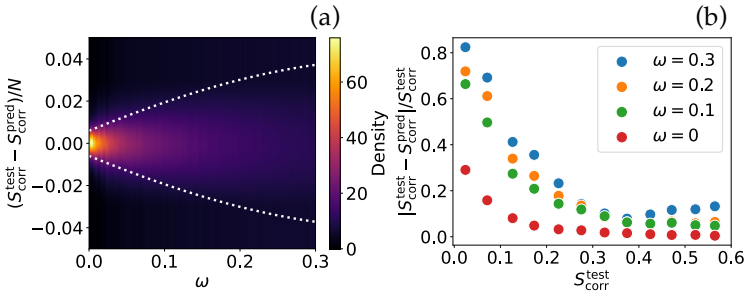

Figure 5: Performance of the neural network model in the presence of strong noise.(a) Probability distribution of the error in the prediction in the presence of noise. (b) Mean absolute percentage error (MAPE) as a function of the degree of correlation. The MAPE has averaged on a small range (0.05) in the values of $S^{\text{test}}_{\text{corr}}$.

References

[1] P. Fulde, *Electron Correlations in Molecules and Solids*, Springer Berlin Heidelberg, doi:10.1007/978-3-642-57809-0 (1995).

[2] P. E. M. Siegbahn, J. Almlöf, A. Heiberg and B. O. Roos, *The complete active space SCF (CASSCF) method in a newton–raphson formulation with application to the HNO molecule*, The Journal of Chemical Physics **74**(4), 2384 (1981), doi:10.1063/1.441359.

[3] M. Debertolis, S. Florens and I. Snyman, *Few-body nature of kondo correlated ground states*, Phys. Rev. B **103**, 235166 (2021), doi:10.1103/PhysRevB.103.235166.

[4] R.-Q. He and Z.-Y. Lu, *Quantum renormalization groups based on natural orbitals*, Phys. Rev. B **89**, 085108 (2014), doi:10.1103/PhysRevB.89.085108.

[5] Y. Lu, M. Höppner, O. Gunnarsson and M. W. Haverkort, *Efficient real-frequency solver for dynamical mean-field theory*, Phys. Rev. B **90**, 085102 (2014), doi:10.1103/PhysRevB.90.085102.

[6] M. T. Fishman and S. R. White, *Compression of correlation matrices and an efficient method for forming matrix product states of fermionic gaussian states*, Phys. Rev. B **92**, 075132 (2015), doi:10.1103/PhysRevB.92.075132.

[7] J. Bardeen, L. N. Cooper and J. R. Schrieffer, *Theory of superconductivity*, Phys. Rev. **108**, 1175 (1957), doi:10.1103/PhysRev.108.1175.

[8] M. Sigrist and K. Ueda, *Phenomenological theory of unconventional superconductivity*, Rev. Mod. Phys. **63**, 239 (1991), doi:10.1103/RevModPhys.63.239.

[9] P. W. Anderson, *The resonating valence bond state in La_2CuO_4 and superconductivity*, Science **235**(4793), 1196 (1987), doi:10.1126/science.235.4793.1196.

[10] L. Savary and L. Balents, *Quantum spin liquids: a review*, Reports on Progress in Physics **80**(1), 016502 (2016), doi:10.1088/0034-4885/80/1/016502.

[11] B. Keimer and J. E. Moore, *The physics of quantum materials*, Nature Physics **13**(11), 1045 (2017), doi:10.1038/nphys4302.

[12] C. N. Lau, F. Xia and L. Cao, *Emergent quantum materials*, MRS Bulletin **45**(5), 340 (2020), doi:10.1557/mrs.2020.125.

[13] O. Gühne and G. Tóth, *Entanglement detection*, Physics Reports **474**(1-6), 1 (2009), doi:10.1016/j.physrep.2009.02.004.

[14] J. Eisert, M. Cramer and M. B. Plenio, *Colloquium: Area laws for the entanglement entropy*, Reviews of Modern Physics **82**(1), 277 (2010), doi:10.1103/revmodphys.82.277.

[15] L. Amico, R. Fazio, A. Osterloh and V. Vedral, *Entanglement in many-body systems*, Reviews of Modern Physics **80**(2), 517 (2008), doi:10.1103/revmodphys.80.517.

[16] R. Horodecki, P. Horodecki, M. Horodecki and K. Horodecki, *Quantum entanglement*, Reviews of Modern Physics **81**(2), 865 (2009), doi:10.1103/revmodphys.81.865.

[17] S.-J. Gu, S.-S. Deng, Y.-Q. Li and H.-Q. Lin, *Entanglement and quantum phase transition in the extended hubbard model*, Physical Review Letters **93**(8) (2004), doi:10.1103/physrevlett.93.086402.

[18] V. E. Korepin, *Universality of entropy scaling in one dimensional gapless models*, Physical Review Letters **92**(9) (2004), doi:10.1103/physrevlett.92.096402.

[19] S.-S. Deng, S.-J. Gu and H.-Q. Lin, *Block-block entanglement and quantum phase transitions in the one-dimensional extended hubbard model*, Physical Review B **74**(4) (2006), doi:10.1103/physrevb.74.045103.

[20] F. Iemini, T. O. Maciel and R. O. Vianna, *Entanglement of indistinguishable particles as a probe for quantum phase transitions in the extended hubbard model*, Physical Review B **92**(7) (2015), doi:10.1103/physrevb.92.075423.

[21] H. Wang and S. Kais, *Quantum entanglement and electron correlation in molecular systems*, Israel Journal of Chemistry **47**(1), 59 (2007), doi:10.1560/ijc.47.1.59.

[22] M. C. Tichy, F. Mintert and A. Buchleitner, *Essential entanglement for atomic and molecular physics*, Journal of Physics B: Atomic, Molecular and Optical Physics **44**(19), 192001 (2011), doi:10.1088/0953-4075/44/19/192001.

[23] T. S. Hofer, *On the basis set convergence of electron–electron entanglement measures: helium-like systems*, Frontiers in Chemistry **1** (2013), doi:10.3389/fchem.2013.00024.

[24] R. O. Esquivel, S. López-Rosa and J. S. Dehesa, *Correlation energy as a measure of non-locality: Quantum entanglement of helium-like systems*, EPL (Europhysics Letters) **111**(4), 40009 (2015), doi:10.1209/0295-5075/111/40009.

[25] R. O. Esquivel, A. L. Rodríguez, R. P. Sagar, M. Hô and V. H. Smith, *Physical interpretation of information entropy: Numerical evidence of the collins conjecture*, Physical Review A **54**(1), 259 (1996), doi:10.1103/physreva.54.259.

[26] P. Gersdorf, W. John, J. P. Perdew and P. Ziesche, *Correlation entropy of the h2 molecule*, International Journal of Quantum Chemistry **61**(6), 935 (1997), doi:10.1002/(sici)1097-461x(1997)61:6<935::aid-qua6>3.0.co;2-x.

[27] P. Ziesche, O. Gunnarsson, W. John and H. Beck, *Two-site hubbard model, the bardeen-cooper-schrieffer model, and the concept of correlation entropy*, Physical Review B **55**(16), 10270 (1997), doi:10.1103/physrevb.55.10270.

[28] Z. Huang, H. Wang and S. Kais, *Entanglement and electron correlation in quantum chemistry calculations*, Journal of Modern Optics **53**(16-17), 2543 (2006), doi:10.1080/09500340600955674.

[29] C. L. Benavides-Riveros, N. N. Lathiotakis, C. Schilling and M. A. L. Marques, *Relating correlation measures: The importance of the energy gap*, Physical Review A **95**(3) (2017), doi:10.1103/physreva.95.032507.

[30] D. L. B. Ferreira, T. O. Maciel, R. O. Vianna and F. Iemini, *Quantum correlations, entanglement spectrum, and coherence of the two-particle reduced density matrix in the extended hubbard model*, Physical Review B **105**(11) (2022), doi:10.1103/physrevb.105.115145.

[31] G. Carleo, I. Cirac, K. Cranmer, L. Daudet, M. Schuld, N. Tishby, L. Vogt-Maranto and L. Zdeborová, *Machine learning and the physical sciences*, Reviews of Modern Physics **91**(4) (2019), doi:10.1103/revmodphys.91.045002.

[32] J. Carrasquilla, *Machine learning for quantum matter*, Advances in Physics: X **5**(1), 1797528 (2020), doi:10.1080/23746149.2020.1797528.

[33] K. Shinjo, K. Sasaki, S. Hase, S. Sota, S. Ejima, S. Yunoki and T. Tohyama, *Machine learning phase diagram in the half-filled one-dimensional extended hubbard model*, Journal of the Physical Society of Japan **88**(6), 065001 (2019), doi:10.7566/jpsj.88.065001.

[34] H. Saito, *Solving the bose–hubbard model with machine learning*, Journal of the Physical Society of Japan **86**(9), 093001 (2017), doi:10.7566/jpsj.86.093001.

[35] V. Dunjko and H. J. Briegel, *Machine learning & artificial intelligence in the quantum domain: a review of recent progress*, Reports on Progress in Physics **81**(7), 074001 (2018), doi:10.1088/1361-6633/aab406.

[36] O. S. Zozulya, M. Haque, K. Schoutens and E. H. Rezayi, *Bipartite entanglement entropy in fractional quantum hall states*, Phys. Rev. B **76**, 125310 (2007), doi:10.1103/PhysRevB.76.125310.

[37] H. Li and F. D. M. Haldane, *Entanglement spectrum as a generalization of entanglement entropy: Identification of topological order in non-abelian fractional quantum hall effect states*, Phys. Rev. Lett. **101**, 010504 (2008), doi:10.1103/PhysRevLett.101.010504.

[38] I. Peschel, *Calculation of reduced density matrices from correlation functions*, Journal of Physics A: Mathematical and General **36**(14), L205 (2003), doi:10.1088/0305-4470/36/14/101.

[39] S. R. White, *Density matrix formulation for quantum renormalization groups*, Phys. Rev. Lett. **69**, 2863 (1992), doi:10.1103/PhysRevLett.69.2863.

[40] M. Fishman, S. R. White and E. Miles Stoudenmire, *The ITensor Software Library for Tensor Network Calculations*, arXiv e-prints arXiv:2007.14822 (2020), 2007.14822.

[41] ITensor Library http://itensor.org .

[42] *DMRGpy library, https://github.com/joselado/dmrgpy*.

[43] A. Anfossi, C. D. E. Boschi, A. Montorsi and F. Ortolani, *Single-site entanglement at the superconductor-insulator transition in the hirsch model*, Physical Review B **73**(8) (2006), doi:10.1103/physrevb.73.085113.

[44] C. Mund, O. Legeza and R. M. Noack, *Quantum information analysis of the phase diagram of the half-filled extended hubbard model*, Physical Review B **79**(24) (2009), doi:10.1103/physrevb.79.245130.

[45] Y.-C. Li and Z.-G. Yuan, *Direct evidence of the BOW and TS states in the half-filled one-dimensional extended hubbard model*, Physics Letters A **380**(1-2), 272 (2016), doi:10.1016/j.physleta.2015.09.034.

[46] C. Walsh, P. Sémon, D. Poulin, G. Sordi and A.-M. Tremblay, *Local entanglement entropy and mutual information across the mott transition in the two-dimensional hubbard model*, Physical Review Letters **122**(6) (2019), doi:10.1103/physrevlett.122.067203.

[47] S. Glocke, A. Klümper and J. Sirker, *Half-filled one-dimensional extended hubbard model: Phase diagram and thermodynamics*, Physical Review B **76**(15) (2007), doi:10.1103/physrevb.76.155121.

[48] G. R. Schleder, A. C. M. Padilha, C. M. Acosta, M. Costa and A. Fazzio, *From DFT to machine learning: recent approaches to materials science–a review*, Journal of Physics: Materials **2**(3), 032001 (2019), doi:10.1088/2515-7639/ab084b.

[49] E. Bedolla, L. C. Padierna and R. Castañeda-Priego, *Machine learning for condensed matter physics*, Journal of Physics: Condensed Matter **33**(5), 053001 (2020), doi:10.1088/1361-648x/abb895.

[50] J. F. Rodriguez-Nieva and M. S. Scheurer, *Identifying topological order through unsupervised machine learning*, Nature Physics **15**(8), 790 (2019), doi:10.1038/s41567-019-0512-x.

[51] P. Baireuther, M. Płodzień, T. Ojanen, J. Tworzydło and T. Hyart, *Identifying Chern numbers of superconductors from local measurements*, arXiv e-prints arXiv:2112.06777 (2021), 2112.06777.

[52] E. Lustig, O. Yair, R. Talmon and M. Segev, *Identifying topological phase transitions in experiments using manifold learning*, Phys. Rev. Lett. **125**, 127401 (2020), doi:10.1103/PhysRevLett.125.127401.

[53] D. Carvalho, N. A. García-Martínez, J. L. Lado and J. Fernández-Rossier, *Real-space mapping of topological invariants using artificial neural networks*, Phys. Rev. B **97**, 115453 (2018), doi:10.1103/PhysRevB.97.115453.

[54] N. L. Holanda and M. A. R. Griffith, *Machine learning topological phases in real space*, Phys. Rev. B **102**, 054107 (2020), doi:10.1103/PhysRevB.102.054107.

[55] R. Islam, R. Ma, P. M. Preiss, M. E. Tai, A. Lukin, M. Rispoli and M. Greiner, *Measuring entanglement entropy in a quantum many-body system*, Nature **528**(7580), 77 (2015), doi:10.1038/nature15750.

[56] A. Bergschneider, V. M. Klinkhamer, J. H. Becher, R. Klemt, L. Palm, G. Zürn, S. Jochim and P. M. Preiss, *Experimental characterization of two-particle entanglement through position and momentum correlations*, Nature Physics **15**(7), 640 (2019), doi:10.1038/s41567-019-0508-6.

[57] A. D. Maestro, H. Barghathi and B. Rosenow, *Measuring postquench entanglement entropy through density correlations*, Physical Review Research **4**(2) (2022), doi:10.1103/physrevresearch.4.l022023.

[58] T. Hensgens, T. Fujita, L. Janssen, X. Li, C. J. V. Diepen, C. Reichl, W. Wegscheider, S. D. Sarma and L. M. K. Vandersypen, *Quantum simulation of a fermi–hubbard model using a semiconductor quantum dot array*, Nature **548**(7665), 70 (2017), doi:10.1038/nature23022.

[59] J. P. Dehollain, U. Mukhopadhyay, V. P. Michal, Y. Wang, B. Wunsch, C. Reichl, W. Wegscheider, M. S. Rudner, E. Demler and L. M. K. Vandersypen, *Nagaoka ferromagnetism observed in a quantum dot plaquette*, Nature **579**(7800), 528 (2020), doi:10.1038/s41586-020-2051-0.

[60] J. R. Hauptmann, J. Paaske and P. E. Lindelof, *Electric-field-controlled spin reversal in a quantum dot with ferromagnetic contacts*, Nature Physics **4**(5), 373 (2008), doi:10.1038/nphys931.

[61] S. Lindebaum, D. Urban and J. König, *Spin-induced charge correlations in transport through interacting quantum dots with ferromagnetic leads*, Phys. Rev. B **79**, 245303 (2009), doi:10.1103/PhysRevB.79.245303.

[62] M. F. Crommie, C. P. Lutz and D. M. Eigler, *Imaging standing waves in a two-dimensional electron gas*, Nature **363**(6429), 524 (1993), doi:10.1038/363524a0.

[63] J. Lee, D. Wong, J. V. Jr, J. F. Rodriguez-Nieva, S. Kahn, H.-Z. Tsai, T. Taniguchi, K. Watanabe, A. Zettl, F. Wang, L. S. Levitov and M. F. Crommie, *Imaging electrostatically confined dirac fermions in graphene quantum dots*, Nature Physics **12**(11), 1032 (2016), doi:10.1038/nphys3805.

[64] B. Sothmann and J. König, *Transport through quantum-dot spin valves containing magnetic impurities*, Phys. Rev. B **82**, 245319 (2010), doi:10.1103/PhysRevB.82.245319.

[65] M. Bouhassoune, B. Zimmermann, P. Mavropoulos, D. Wortmann, P. H. Dederichs, S. Blügel and S. Lounis, *Quantum well states and amplified spin-dependent friedel oscillations in thin films*, Nature Communications **5**(1) (2014), doi:10.1038/ncomms6558.

[66] F. Chollet *et al.*, *Keras*, https://keras.io (2015).

[67] *Code and data of the work available in https://zenodo.org/record/6611506*.

[68] U. Schollwöck, *The density-matrix renormalization group in the age of matrix product states*, Annals of Physics **326**(1), 96 (2011), doi:10.1016/j.aop.2010.09.012.